Geoenvironmental Disasters

RESEARCH Open Access

Investigation of offshore landslides impact on bucket foundations using a coupled SPH–FEM method

Zehao Wang[1], Defeng Zheng[2], Xingsen Guo[3*], Zhongde Gu[1], Yueqiang Shen[1] and Tingkai Nian[1*]

Abstract

Background As the exploitation of marine resources intensifies, the impact of submarine landslides on underwater structures has become a significant issue. Existing research primarily focuses on the impact on pipelines, often neglecting the actual deformation and mechanical response of underwater structures under impact loads in numerical simulations, thus complicating the evaluation of the reliability of these engineering structures in extreme conditions. Moreover, the dynamic response of bucket foundations, a common form of underwater base, under the effect of submarine landslide impacts remains unclear.

Methods To address this knowledge gap, we have developed a fluid-structure coupling system that employs the coupled Smoothed Particle Hydrodynamics (SPH)-Finite Element Method (FEM) to investigate a single impact process and analyze the displacement response of bucket foundations within a water-offshore landslide-bucket foundationsubgrade context. The accuracy of this developed method has been systematically verified through comparisons with previous experimental and numerical results.

Results During a submarine landslide impact event, the impact force demonstrates a distinct decrease followed by stabilization, and the displacement response of the bucket foundation exhibits a rebound effect after reaching its maximum value. Furthermore, we conducted an extensive analysis of different impact angles for underwater data centers equipped with multi-bucket foundations. Our study revealed that group-bucket foundations experience a combined translation-turnover failure when subjected to submarine landslide impacts, and the most unfavorable scenario for such impact is identified. The research introduces a novel numerical simulation approach for investigating the impact of submarine landslides on complex underwater structures.

Keywords Offshore landslide, Coupled SPH-FEM method, Impact effect, Bucket foundation, Underwater data center

Introduction

In recent years, the development of offshore wind power and oil platforms has led to significant advancements in bucket foundations. Compared to traditional offshore foundations, the bucket foundation possesses unique advantages during construction and operation (Gao et al. 2021), making them highly promising for various applications and attracting considerable attention from both academia and industry. However, more frequent extreme marine events are increasing geological hazards, such as seabed instability and submarine landslides

*Correspondence:
Xingsen Guo
xingsen.guo@ucl.ac.uk
Tingkai Nian
tknian@dlut.edu.cn
[1] State Key Laboratory of Coastal and Offshore Engineering, Dalian University of Technology, Dalian 116024, China
[2] Liaoning Key Laboratory of Physical Geography and Geomatics Science, Liaoning Normal University, Dalian 116029, China
[3] Department of Civil, Environmental, and Geomatic Engineering, University College London, London WC1E 6BT, UK

© The Author(s) 2024. **Open Access** This article is licensed under a Creative Commons Attribution 4.0 International License, which permits use, sharing, adaptation, distribution and reproduction in any medium or format, as long as you give appropriate credit to the original author(s) and the source, provide a link to the Creative Commons licence, and indicate if changes were made. The images or other third party material in this article are included in the article's Creative Commons licence, unless indicated otherwise in a credit line to the material. If material is not included in the article's Creative Commons licence and your intended use is not permitted by statutory regulation or exceeds the permitted use, you will need to obtain permission directly from the copyright holder. To view a copy of this licence, visit http://creativecommons.org/licenses/by/4.0/.

Content courtesy of Springer Nature, terms of use apply. Rights reserved.

caused by offshore storm surges, submarine earthquakes, hydrate decomposition, and human engineering activities (Sun and Bolin 2014; El Talibi et al. 2016; Nian et al. 2019; Khalfaoui et al. 2020; Shano et al. 2020; Zheng et al. 2021; Liu et al. 2023; Guo et al. 2023). These incidents have had a significant impact on underwater facilities in offshore engineering, leading to severe loss of life and property. For instance, in 1969, Hurricane Camille triggered a submarine landslide that damaged three offshore oil platforms in the Mississippi Delta, causing substantial economic losses (Bea 1971). In March 1977, an underwater oil pipeline belonging to Texaco in the United States was damaged by a submarine landslide, leading to a massive oil spillage (Camargo et al. 2019; Zhao et al. 2021). In 2006, 2009, and 2010, submarine landslides destroyed the underwater cables in the Luzon Strait multiple times, disrupting communications between Southeast Asian countries and China for up to 12 h (Hsu et al. 2008). Over the past 30 years, the Chinese Chengdao offshore oil field has experienced seven platform tilting incidents, seventeen cable failure incidents, and two submarine pipeline rupture incidents, all of which were speculated to be related to the destabilization of submarine sediments (Wang et al. 2020). Given the limited understanding of the mechanical behavior of bucket foundations under catastrophic loads of submarine landslides, it is crucial to conduct comprehensive research on the influence of offshore landslides on bucket foundations.

Currently, the study of landslide impact on underwater infrastructure heavily relies on numerical simulations, with Computational Fluid Dynamics (CFD) being widely used (Zakeri et al. 2009; Liu et al. 2015; Nian et al. 2018; Dutta and Hawlader 2019; Guo et al. 2019, 2021, 2022a, 2022b; Qian et al. 2020, 2023; Fan et al. 2022). In these simulations, various predictive models have been developed to assess the forces acting on underwater structures subjected to landslide impacts. However, these simulations often treat the structures (e.g., piles, pipelines) as fixed boundary walls, neglecting the actual deformation and mechanical response of underwater structures under impact loads, which makes it challenging to evaluate the reliability of these engineering structures under extreme conditions (Dong et al. 2017; Nian et al. 2018; Dutta and Hawlader 2019; Guo et al. 2019; Guo et al. 2022a, b; Qian et al. 2023). Additionally, these studies often simulate the instantaneous impact of homogeneous landslide bodies on underwater structures (Zakeri et al. 2009; Nian et al. 2018; Guo et al. 2021), neglecting the morphological evolution of the landslide's leading edge during the pre-impact transportation process, which makes it deviates from the actual morphology of offshore landslides. In recent years, meshless methods, such as Smoothed Particle Hydrodynamics (SPH), have gained increasing popularity in geotechnical engineering studies (Dai et al. 2017; Zhang et al. 2019; Feng et al. 2022). The SPH method offers significant advantages in simulating the discontinuous deformation and large-deformation flow of soils (Chen and Yan 2021), as it does not rely on the assumption of macroscopic continuum media. On the other hand, the Finite Element Method (FEM) has achieved remarkable results in simulating structural deformations. Therefore, the coupling of these two methods within the Lagrangian framework can simulate the bidirectional fluid–structure coupling between underwater landslide (SPH particles) and bucket foundations (FEM). This allows for the determination of the dynamic displacement response of underwater foundations during landslide impact events. Furthermore, by incorporating Finite Element contact interactions between bucket foundations and the subgrade throughout the impact process, we can characterize the instability characteristics of underwater foundations subjected to impact loads. Hence, the SPH-FEM coupling method exhibits substantial potential to emerge as a robust approach for addressing the aforementioned challenges. However, there is limited research specifically focusing on the application of the coupled SPH-FEM method to investigate the impact of submarine landslides on underwater infrastructures (Luo et al. 2019).

To address this research gap, this study introduces the coupled SPH-FEM method, establishes a three-dimensional fluid–structure coupling system of the water-landslide body-bucket foundation-subgrade, quantifies the dynamic response of the underwater foundation, and explores the effect of different variables on the bucket foundation and the underwater data center. The research aims to elucidate bucket foundations' operational performance and mechanical behavior when subjected to offshore landslides, ensuring safety and reliability throughout their service life.

Coupled SPH-FEM method

Smoothed particle hydrodynamics method

As a fully Lagrangian method, the SPH method discretizes the original continuum by interpolating the values of variables, thus mitigating issues associated with mesh entanglement, distortion, and deformation in FE meshes. The SPH method utilizes integral interpolation to approximate the field variables $f(x)$ (such as temperature, stress, density, etc.) at any given point. In this method, the value of a variable associated with a key particle x_i is approximated by taking the mean value of contributions from a set of neighboring particles x_j (Monaghan 1992), as given in Eq. (1).

$$f(x_i,t)=\int_V f(x_j,t)W(x_i-x_j,h)\mathrm{d}V \tag{1}$$

Content courtesy of Springer Nature, terms of use apply. Rights reserved.

where x_i is the focal particle, x_j is the neighboring particles, t is the time, V is the support domain; $W(x_i - x_j, h)$ is the kernel function, and h is the unit smooth length, defining the region of influence of the kernel function. The support domain is discretized into particles, and then a weighted summation is performed by considering all particles (Monaghan 1992), as given in Eq. (2).

$$\begin{aligned} f(x_i,t) &= \sum_j f(x_j,t)W(x_i - x_j,h)\Delta V_j \\ &= \sum_j f(x_j,t)W(x_i - x_j,h)\frac{m_j}{\rho_j} \end{aligned} \tag{2}$$

where ΔV_j is the volume occupied by particle j, which can be calculated from m_j / ρ_j. Typically, it is necessary to differentiate the field variables (Monaghan 1992), as given in Eq. (3).

$$\nabla f(x_i,t) = \sum_j f(x_j,t)\frac{m_j}{\rho_j}\nabla W(x_i - x_j,h) \tag{3}$$

Since the variables f, m, and ρ are constant for a specific particle, solving for the gradient of the field variable can be transformed into solving for the gradient of the kernel function, thus avoiding the need for grid differencing. If the smoothing length for a particle is denoted as h, then the domain of the kernel function lies within a circle centered at the particle, with a radius of kh, which represents the smoothing length. The definition of the kernel function must satisfy various conditions. In this study, we illustrate the example of a cubic spline kernel (Monaghan 1994), as given in Eq. (4).

$$W(x_i - x_j,h) = \frac{3}{2\pi h^3}\begin{cases} \frac{1}{2}\left(\frac{x_i - x_j}{h}\right)^3 - \left(\frac{x_i - x_j}{h}\right)^2 + \frac{2}{3} & 0 \le \frac{x_i - x_j}{h} \le 1 \\ \frac{1}{6}\left(2 - \frac{x_i - x_j}{h}\right)^3 & 1 \le \frac{x_i - x_j}{h} \le 2 \end{cases} \tag{4}$$

where $x_i - x_j$ represents the relative distance between particles, defined by the particleization. The coupling between SPH particles is achieved by interpolation of the kernel function (i.e., SPH particles of different materials are considered as the same component, and a weighted sum is calculated for all particles within the smooth radius). To simulate the motion of fluids using the particle method, the motion state of particles needs to satisfy the fluid motion equations, namely the conservation of mass equation and the momentum equation (Monaghan 2002), which can be expressed in Eqs. (5), Eq. (6):

$$\frac{\mathrm{d}\rho_i}{\mathrm{d}t} = \rho_i \sum_j \frac{m_j}{\rho_j}(v_i - v_j)\cdot\nabla_i W_{ij} \tag{5}$$

$$\frac{\mathrm{d}v_i}{\mathrm{d}t} = -\sum_j m_j\left(\frac{p_i}{\rho_i^2} + \frac{p_j}{\rho_j^2}\right)\nabla_i W_{ij} - g \tag{6}$$

where v is the velocity, p is the pressure, g is the gravitational acceleration. Noting that ∇_i adheres to the summation convention. The motion of fluid particles is induced by the pressure field gradient, governed by the equation of state. Taking an example of the linear Us-Up Hugoniot form mentioned in this paper, the pressure p can be represented in Eq. (7):

$$p = \frac{\rho_0 c_0^2 \eta}{(1 - s\eta)^2}\left(1 - \frac{\Gamma_0\eta}{2}\right) + \Gamma_0\rho_0 E_m \tag{7}$$

where Us represents the shock velocity, Up is the particle velocity, η is the nominal volumetric compressive strain,

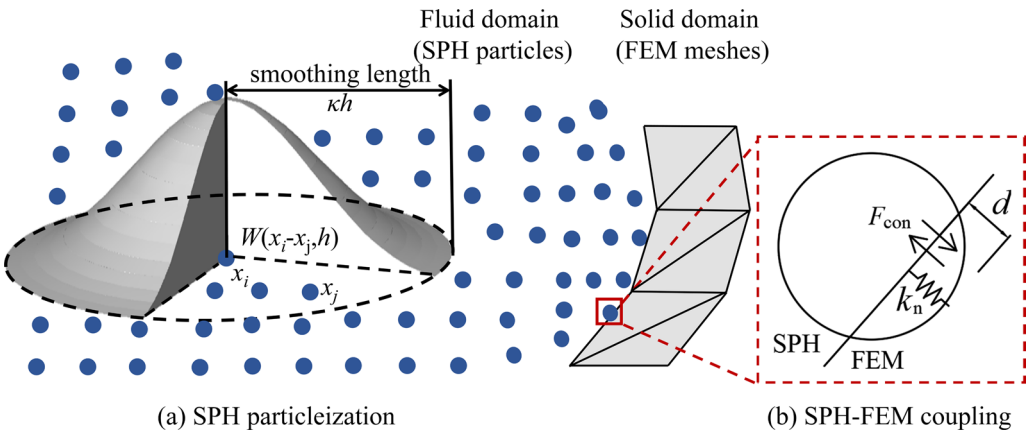

Fig. 1 The proposed SPH-FEM coupling method

Content courtesy of Springer Nature, terms of use apply. Rights reserved.

c_0 is the bulk speed of sound, as the intercept of the linear Us-Up form and s is the slope, E_m is the initial value of specific energy and Γ_0 is the Grüneisen ratio.

Coupling algorithm

In the SPH-FEM coupling algorithm (shown in Fig. 1), a node-to-surface penalty contact algorithm is typically adopted to enforce balance and coordination conditions at the interface between the fluid and solid phases (Attaway et al. 1994; Campbell et al. 2000). Therein, SPH particles act as a node-based surface with a contact thickness equal to the characteristic length l_0, while FE meshes serve as an element-based surface. It is worth noting that l_0 determines the collision volume size for each SPH particle. When discretizing the continuum, it is advisable to set l_0 as half of the initial gap distance, ensuring that all particles are initially in exact contact, thus avoiding the pressure fluctuation effect caused by the initial particle overlay (Huang and Zhu 2015; Zhan et al. 2020). For each SPH particle in the fluid domain, the contact algorithm automatically checks for any penetration of a node into the main surface. Upon detecting penetration, a penalty contact force is introduced simultaneously to both SPH particles and FE meshes to ensure that fluid particles cannot penetrate the solid elements. The contact force $\boldsymbol{F}_{\text{con}}$ comprises both normal and tangential components, as given in Eqs. (8)–(10):

$$\boldsymbol{F}_{\text{con}}^{n} = -k_{\text{n}} d\boldsymbol{n} \tag{8}$$

$$\boldsymbol{F}_{\text{con}}^{\tau} = \alpha \cdot k\left(\frac{\partial \boldsymbol{u}_{\text{FEM}}}{\partial t} - \boldsymbol{v}\right) \tag{9}$$

$$\boldsymbol{F}_{\text{con}} = \boldsymbol{F}_{\text{con}}^{n} + \boldsymbol{F}_{\text{con}}^{\tau} \tag{10}$$

where $\boldsymbol{F}_{\text{con}}^{n}$ is the normal contact force, d is the penetration depth, k_{n} is the main surface stiffness factor, $\boldsymbol{n}$ is the normal vector of the element at the boundary, $\boldsymbol{F}_{\text{con}}^{\tau}$ is the tangential contact force, α is a coefficient, k is the friction coefficient, $\boldsymbol{u}_{\text{FEM}}$ is the displacement of nodes at the boundary, t is the time, and $\boldsymbol{v}$ is the velocity of SPH particles. The main surface stiffness factor k_{n} is related to the stable time Increment of the explicit computation Δt_{stable}, as given in Eq. (11).

$$k_{\text{n}} = \frac{1}{(\Delta t_{\text{stable}})^2} \frac{m_n}{m_i + m_n} \tag{11}$$

where m_i is the mass of particles, and m_n is the nodal mass associated with the master segment. $\boldsymbol{F}_{\text{con}}$ establishes the correlation between the acceleration of SPH particles and the stress–strain of FE meshes. The stable time increment Δt_{stable} is given by:

$$\Delta t_{\text{stable}} = \min\left\{\Delta t_{\text{stable}}^{\text{FEM}}, \Delta t_{\text{stable}}^{\text{SPH}}\right\} \tag{12}$$

$$\Delta t_{\text{stable}}^{\text{FEM}} = \min\left\{\frac{\lambda L}{\sqrt{E(1-\nu)/\rho(1+\nu)(1+2\nu)}}\right\} \tag{13}$$

$$\Delta t_{\text{stable}}^{\text{SPH}} = \min\left\{\lambda' \cdot \sqrt{\frac{h}{\mathrm{d}v/\mathrm{d}t}}\right\} \tag{14}$$

where $\Delta t_{\text{stable}}^{\text{FEM}}$ is the stable time increment of FE meshes, $\Delta t_{\text{stable}}^{\text{FEM}}$ is the stable time increment of SPH particles, λ and λ' remain constant and are generally taken as $0.8 \sim 0.98$, L is the length of elements, E is the elastic bulk modulus, υ is the passion ratio and ρ is the density. The velocity of SPH particles and the position of FE meshes in the subsequent increment are updated, to achieve coupling between the two methods. The coupling of the SPH method and FEM is executed within ABAQUS environment and its flowchart is shown in Fig. 2 (Liang and Chen 2019).

Validation of the numerical method

Validation of fluid motion patterns

To validate the proposed SPH-FEM coupling method, a three-dimensional fluid–structure interaction experiment [i.e., the ETSIN experiment (Lobovský et al. 2014)] is simulated. The experimental setup consisted of a water tank divided into two sections by a movable gate, as shown in Fig. 3. The tank's side walls and the gate were both made of PMMA plates. When the gate was lifted, a dam-break flow occurred, impacting the left side wall. This problem involved significant fluid deformation, splashing, and reflow after impact, which helped validate the accuracy and robustness of the numerical methods.

In the SPH-FEM numerical model, the sidewalls are linearly elastic and modeled using FE meshes, with a density $\rho = 1.19$ g/cm^3, an elastic modulus $E = 3.2$ GPa, and a Poisson's ratio $\nu = 0.32$ (Ucar et al. 2012). The fluid is modeled using 30256 SPH particles, with a characteristic length $l_0 = 5$ mm and a cubic kernel function, which mitigates potential numerical instabilities (Xu and Kikuchi 2005). The smoothing length factor varies with the velocity field but is restricted to ensure that the number of particles associated with a single SPH particle is less than 140 for computational efficiency. The fluid follows the Us-Up model, with a sound speed in water $c_0 = 1450$ m/s and a dynamic viscosity $\mu = 8.87 \times 10^{-4}$ Pa·s (Zhu and Fei 2022). Frictionless rigid contact is assumed between the fluid and the FE meshes.

Content courtesy of Springer Nature, terms of use apply. Rights reserved.

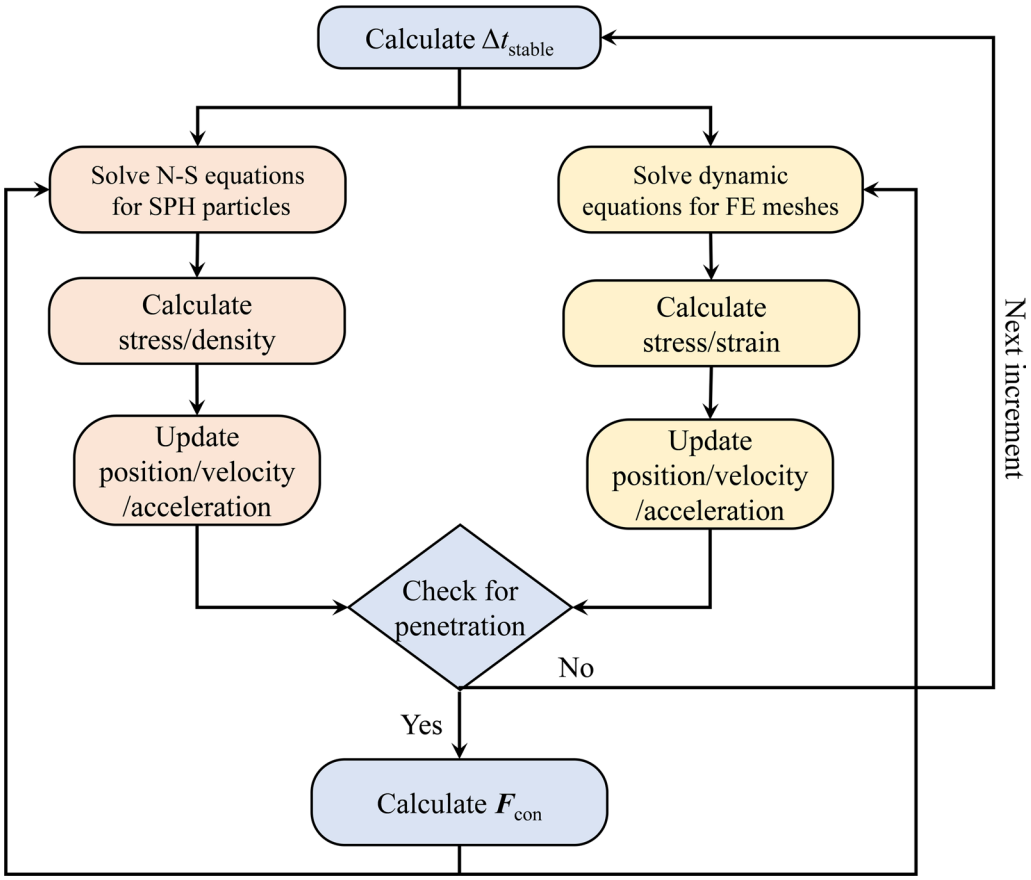

Fig. 2 The flowchart of the coupled SPH-FEM method (modified from Liang and Chen 2019)

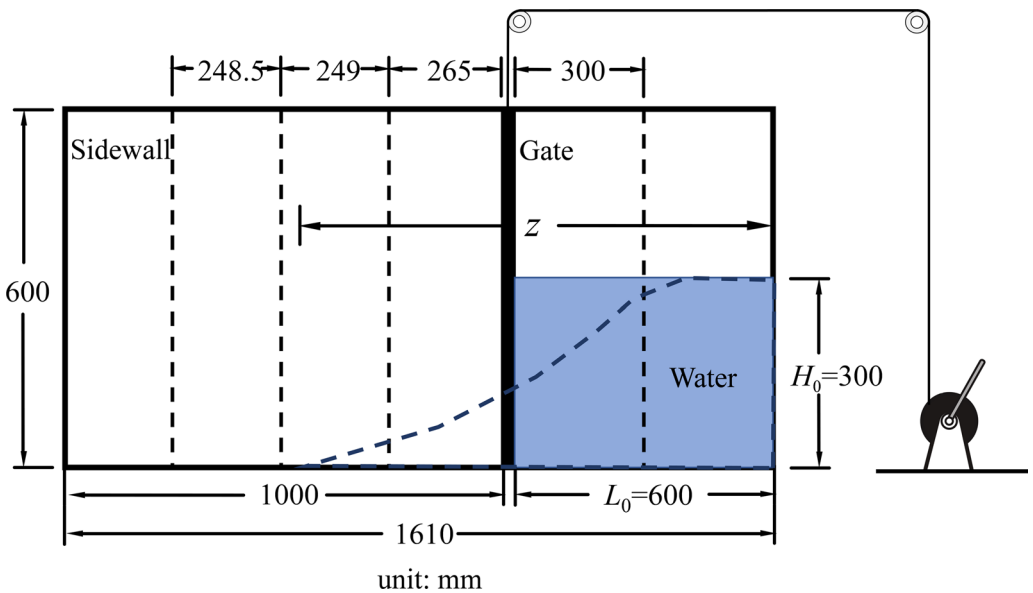

Fig. 3 Schematic diagram of the side view of the ETSIN test (modified from Lobovský et al. 2014)

Content courtesy of Springer Nature, terms of use apply. Rights reserved.

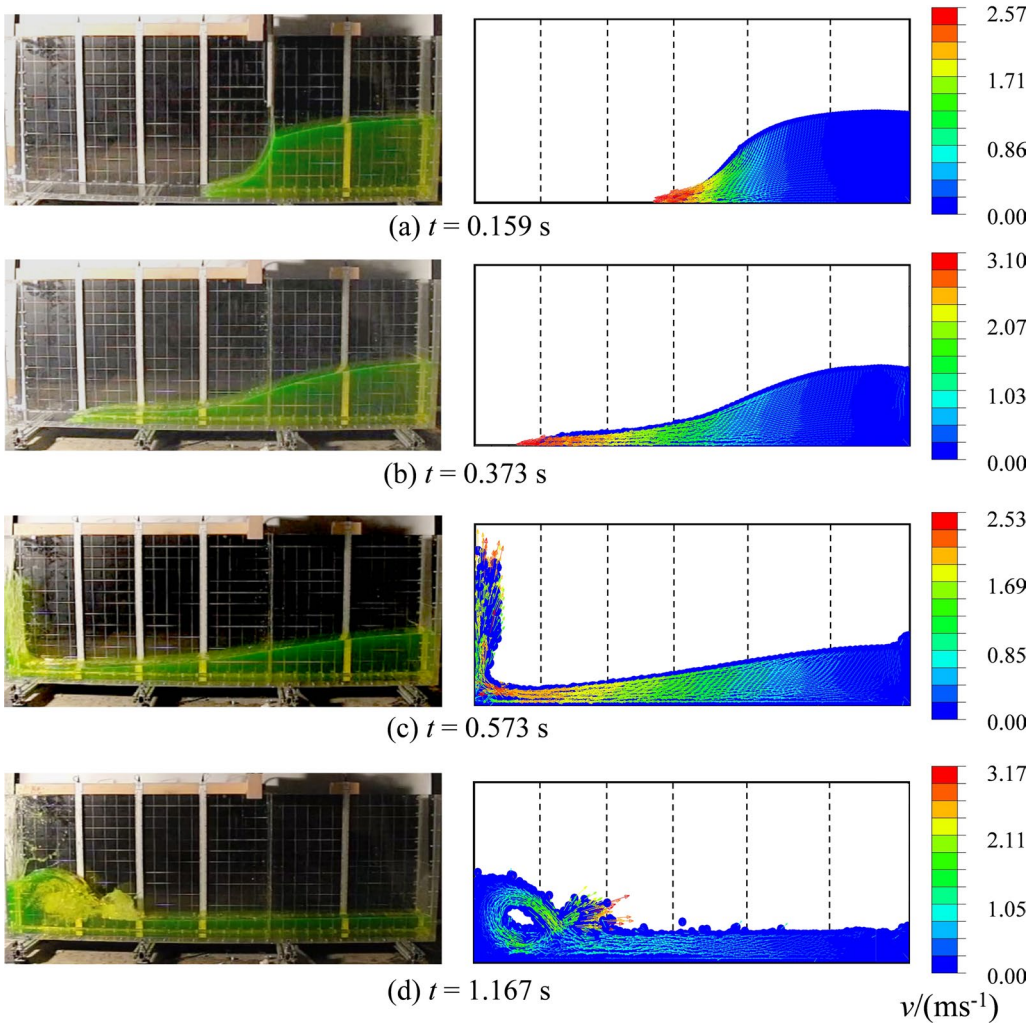

Fig. 4 Experimental and numerical comparison of fluid morphology (Left: Photos from the ETSIN test (modified from Lobovský et al. 2014); Right: Fluid particle velocity vector using SPH-FEM)

The comparative results are presented in Fig. 4, showing that the experimental and numerical results are consistent in terms of the fluid's morphological characteristics. Additionally, the nondimensionalized position of the fluid leading edge z/H_0 before impact is plotted in Fig. 5, comparing the proposed SPH-FEM method with the original and modified Moving Particle Semi-implicit (MPS) method (Koshizuka and Oka 1996; Zhu et al. 2021). The results demonstrate that the SPH-FEM method closely simulates the movement pattern of the fluid leading edge. Therefore, the utilization of the SPH-FEM method for simulating free surface flow and high-velocity impact problems is feasible and yields accurate results. It's important to note that when simulating the 0.43-s dam break process on a personal computer with an Intel i5-8300H CPU running at 3.8 GHz and 16 GB of RAM, it took 145 s of wall-clock time (using 143098 increments) to complete the simulation with a stabilization time increment of $t_{\text{stable}} = 2 \times 10^{-6}$ s. The computation was achieved through a four-core parallel computing framework within ABAQUS.

Validation of the landslide impact load

Furthermore, a quantitative validation of the fluid's impact load on the underwater pipeline (Dong et al. 2017) is conducted. In this case, the flow-like landslide has a density $\rho = 1500$ kg/m^3, with a length of 28 m and a height of 6 m. It moves with an initial velocity $v_0 = 6$ m/s in the rightward direction, ultimately colliding with a fixed pipeline (shown in Fig. 6). The pipeline is smooth in contact, with a diameter $D = 0.8$ m and a burial depth of 0.4 m. The initial gap between the landslide body and the pipeline is 0.01 m.

Content courtesy of Springer Nature, terms of use apply. Rights reserved.

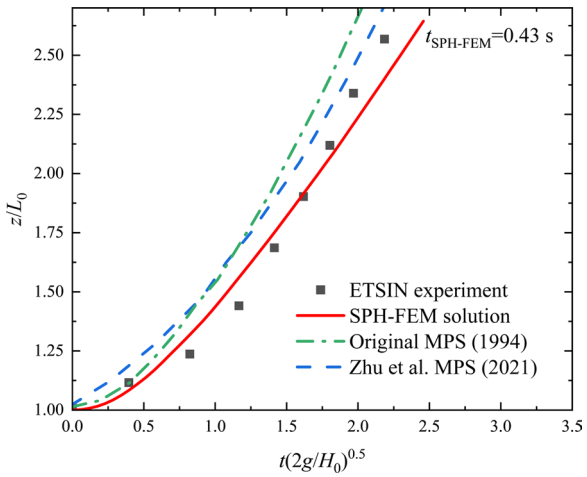

Fig. 5 Comparison of the propagation of fluid frontal motion by different methods (where z represents the horizontal position of the fluid leading edge in Fig. 3, L_0 is the initial length of the fluid, t is the time, g is the gravity acceleration, and H_0 is the initial height of the fluid)

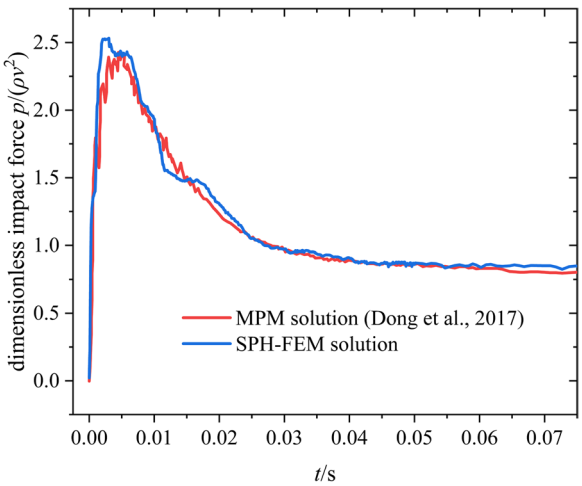

Fig. 7 Comparison of normalized impact force–time curves

In the coupled SPH-FEM model, the rheological characteristics of the landslide are portrayed utilizing a Herschel-Bulkley model, wherein $\tau = 500 + 429.74\ \gamma^{0.23}$ Pa. The characteristic length of the SPH particles is set as $l_0 = 0.05$ m, making a total of 16,800 particles. The pressure p exerted on the pipeline is extracted and normalized to the dimensionless impact force $p/(\rho v^2)$, where v represents the current velocity. The resulting normalized impact force–time history curve is shown in Fig. 7, compared to the MPM method. The results demonstrate that the impact force-time profile obtained from the SPH-FEM simulation closely aligns with the MPM results, exhibiting errors in both peak and steady-state impact forces of less than 5%. Figure 8 displays the velocity vector distribution of particles near the pipeline at $t = 0.12$ s obtained by the proposed SPH-FEM method, along with a comparison to the MPM method. The results demonstrate a strong agreement between the two methods in simulating the morphology of the landslide body. Based on the comparative analysis, it can be concluded that the coupled SPH-FEM method proposed in this study is well-suited for simulating the impact of underwater structures caused by submarine landslides.

Numerical analysis of landslide impact on bucket foundation

Modelling and simulated working conditions

Given the low occurrence rate of large-scale submarine landslides in offshore environments, our study focuses on investigating small-scale landslides without subsequent sediment supply. On the basis of representing the morphology of the landslide's leading edge, the dynamic response of the bucket foundation is accurately examined. The landslide body, initially inclined at a slope angle

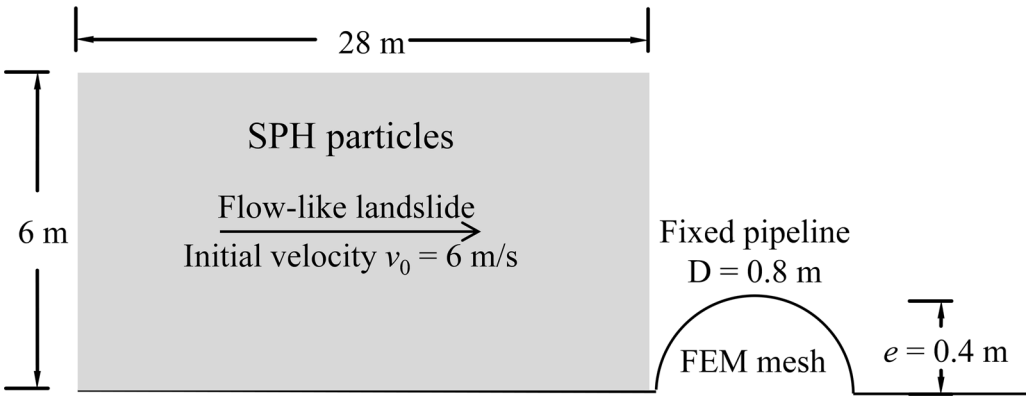

Fig. 6 Schematic diagram of submarine landslide impact semi-buried fixed pipeline (modified from Dong et al. 2017)

Content courtesy of Springer Nature, terms of use apply. Rights reserved.

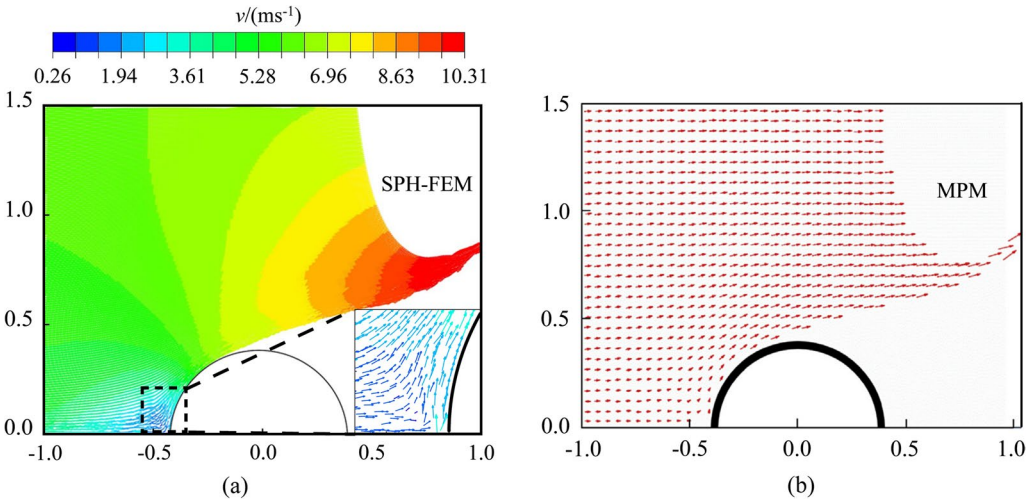

Fig. 8 Comparative analysis of slide morphology at $t = 0.12$ s; **a** SPH-FEM solution; **b** MPM solution (modified from Dong et al. 2017)

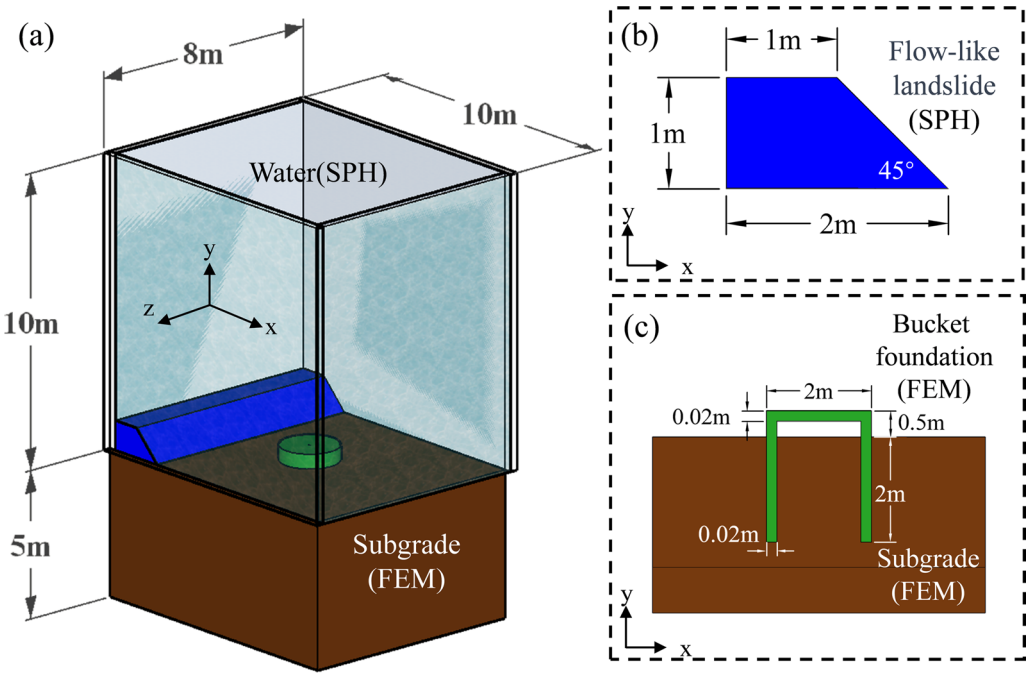

Fig. 9 Numerical modeling of a bucket foundation impacted by an offshore landslide; **a** The whole computational model; **b** The cross-sectional diagram of the landslide; **c** The cross-sectional diagram of the bucket foundation and subgrade

of 45°, has a height of 1 m and a length of 8 m. It is positioned 2 m away from the foundation and exhibits an initial velocity of $v_0 = 5$ m/s in the x-direction (as shown in Fig. 9b). The bucket foundation has a radius of 1 m, a burial depth of 2 m, a wall thickness of 20 mm, and a top plate positioned 0.5 m above the mud surface (as shown in Fig. 9c). The subgrade soil is assumed to be saturated and undrained cohesive soil due to its low permeability, and water pressure from the overlying water body is disregarded. The subgrade adopts an ideal elastoplastic constitutive model based on the Mohr–Coulomb failure criterion, with an undrained strength $s_u = 9.54$ kPa, an elastic modulus $E_s = 500 s_u$, and a Poisson's ratio $\nu_s = 0.49$. The remaining region of the model is filled with overlying water, which interacts with the landslide through interpolation using the kernel function. To accurately simulate the self-weight stress of the bucket foundation under normal service conditions and achieve a balance

Content courtesy of Springer Nature, terms of use apply. Rights reserved.

between internal and external water pressures, a surface load equal to the external water pressure is applied to the interior of the bucket foundation.

The steel bucket foundation is modeled as linear elastic with an average grid size of 0.02 m, while the subgrade adopts a grid size around the bucket of 0.01 m. The mechanical properties of the landslide body are quantified using the Herschel–Bulkley model (Coussot et al. 1998), while the ambient water is treated as a Newtonian fluid, following the Us-Up model. Both the landslide body and water are modeled using SPH particles, with a characteristic length equal to 0.02 m. Cubic splines are employed as kernel functions, and the smoothing length factor is adjusted based on the expansion and compression trends of the model. To mitigate the occurrence of numerical oscillations in variables throughout the impact, the infinite element and Rayleigh damping are implemented. The numerical model parameters are summarized in Table 1 (Korson et al. 1969; Shi et al. 1999; Zakeri et al. 2008; Zhu and Fei 2022).

Results and analysis

Figure 10 depicts the time history curves of the impact force on the bucket foundation by the landslide body and the displacement response of the bucket foundation, wherein the impact force is calculated based on the contact force between the slide and the bucket foundation, and the displacement response is quantified by the maximum horizontal displacement (relative to the initial position) of the bucket foundation. Figure 11 shows the

Table 1 Model parameters

Object	Parameter	Value	Unit
Flow-like landslide	Density ρ_l	1681	kg/m^3
	Shear stress τ	$7.3+3\dot{\gamma}^{0.35}$	Pa
Water	Density ρ_w	1000	kg/m^3
	Dynamic viscosity μ_w	0.0015	Pa·s
	Sound speed c_0	1450	m/s
	Slope of Us-Up form s	0	–
	Grüneisen ratio Γ_0	0	–
Subgrade	Effective density ρ'	846	kg/m^3
	Bulk modulus E_s	2862	kPa
	Poisson's ratio v_s	0.49	
	Cohesive strength c_s	9.54	kPa
Bucket foundation	Density ρ_b	7850	kg/m^3
	Bulk modulus E_b	210	GPa
	Poisson's ratio v_b	0.28	–
	Coefficient of friction k_b	0.328	–

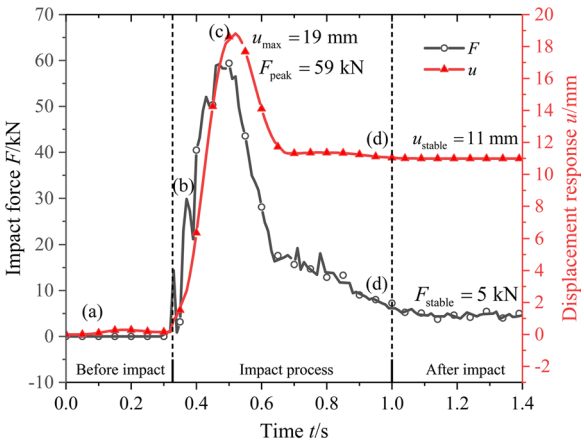

Fig. 10 Impact force and base response curve of the slide body

morphological characteristics and velocity vectors of the landslide body at different times.

It can be observed that during the motion of a landslide approaching a bucket foundation, the particles involved undergo collapse due to their self-weight, resulting in a decrease in the height and slope angle. When the leading edge of the landslide body makes contact with the bucket foundation (t=0.35 s), the velocity of particles rapidly decreases, leading to an increase in impact force and displacement response. The particles flow over the top and around the sides of the bucket foundation. At t=0.49 s, the force exerted on the foundation reaches its peak F_{peak}=59 kN, followed by a maximum displacement response u_{stable}=19 mm (at t=0.51 s). As the kinetic energy of the landslide body dissipates, the velocity of the landslide decreases and stabilizes. At t=1.00 s, the impact force on the bucket foundation gradually diminishes and eventually reaches a steady value of 5 kN, which can be considered as the soil pressure of the landslide mass deposited behind the foundation. The displacement response of the bucket foundation returns to 11 mm, due to the plastic deformation of the subgrade. At this stage,

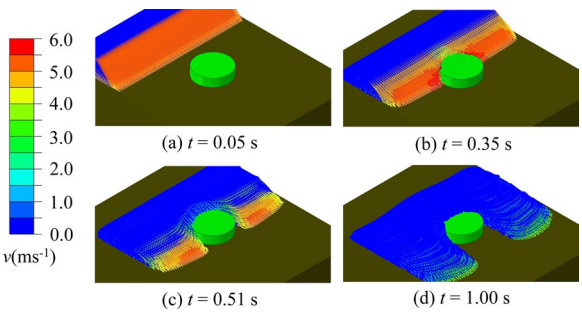

Fig. 11 Morphological characteristics and velocity vectors of slides at different moments

Content courtesy of Springer Nature, terms of use apply. Rights reserved.

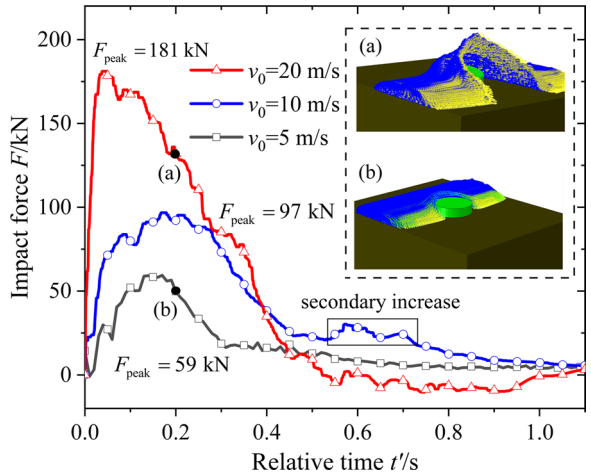

Fig. 12 Impact of slides with different initial velocities on buckets: **a** the velocity vector of the landslide body at t' = 0.2 s with v_0 = 20 m/s; **b** the velocity vector of the landslide body at t' = 0.2 s with v_0 = 5 m/s

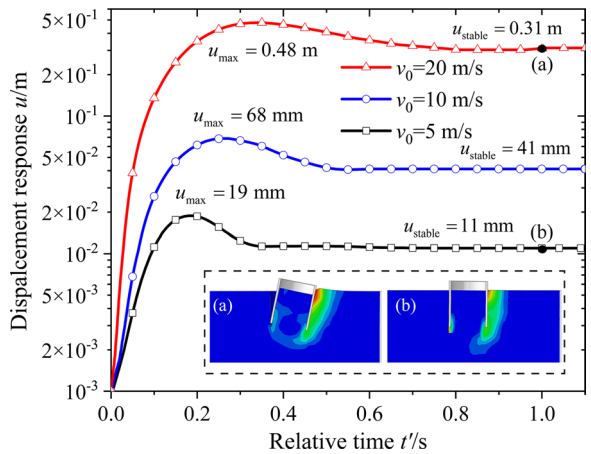

Fig. 13 Displacement response of buckets under the impact of landslides with different velocities; **a** distribution of plastic deformation of subgrade at t' = 1.0 s with v_0 = 20 m/s; **b** distribution of plastic deformation of subgrade at t' = 1.0 s with v_0 = 5 m/s

the impact behavior of the submarine landslide on the bucket foundation has essentially reached a stable state.

Discussions

Considering the uncertainty of offshore landslides, a variable parameter analysis is conducted by selecting 3 key indicators: velocity and thickness of landslide body and the shear strength of subgrade, aiming to uncover the impact effect patterns of offshore landslides on bucket foundations and to elucidate the underlying mechanisms influencing the disaster process.

Effect of velocity

By setting the initial velocities to 5 m/s, 10 m/s, and 20 m/s, the effect of velocity on the impact effect was studied. To ensure a consistent average thickness of the landslide at the moment of impact (H'), the initial spacing was adjusted accordingly. Figure 12 represents the evaluation of impact force, while Fig. 13 depicts the displacement response of the bucket foundation. As the velocity increases, both the impact force and displacement response show a substantial increase. For v_0 = 5 m/s, the slides demonstrate blocking behavior, impeding the flow around the sides and top of the bucket foundation, resulting in a material accumulation at the rear of the bucket. During the process, the impact force exhibits a typical pattern of an increase-peak-decrease-stabilization process. For v_0 = 10 m/s, the flow-like slide around the bucket foundation maintains a higher velocity, resulting in a detachment of the landslide. The peak force duration is relatively long, and an additional secondary increase can be observed. For v_0 = 20 m/s, the SPH particles disperse instantaneously, forming a continuous surface that envelops the bucket foundation. During the process, the maximum instantaneous impact force reaches 181 kN, with a brief duration and eventually oscillating near zero. Notably, the soil in the rear of the bucket experiences cracks development in the active zone, while the passive zone at the front bulges, resulting in the formation of a distinct spoon-shaped penetration zone at the bottom, as shown in Fig. 13(a). Landslides with different velocities exhibit diverse motion behaviors, which significantly affect the pattern of impact force.

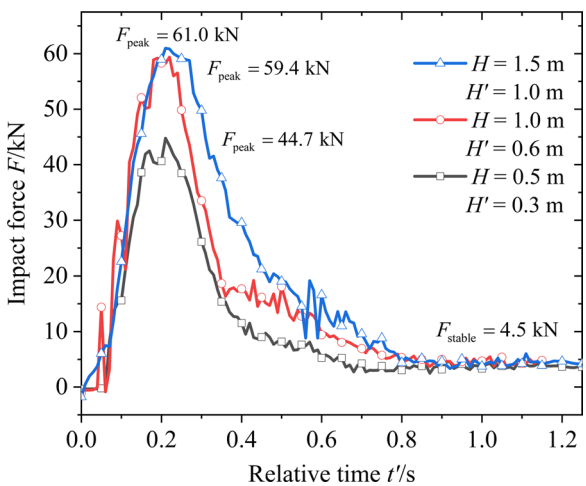

Fig. 14 Impact of slides with different initial thicknesses on buckets

Content courtesy of Springer Nature, terms of use apply. Rights reserved.

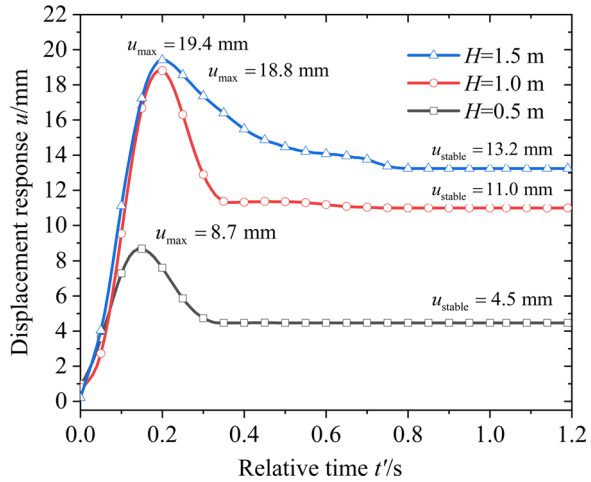

Fig. 15 Displacement response of buckets under the impact of landslides with different thicknesses

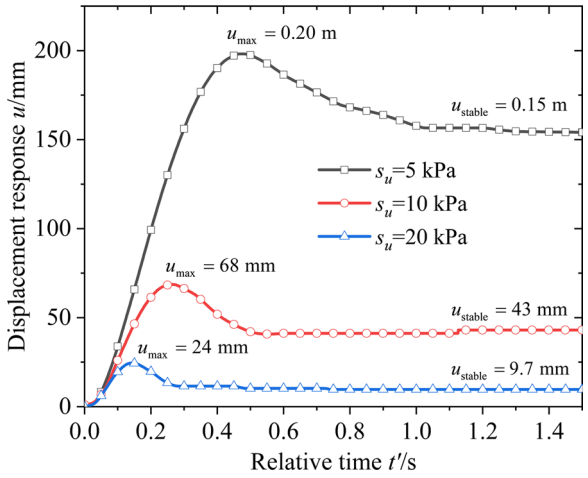

Fig. 17 Effect of different subgrade soil shear strength on the displacement response

Effect of thickness

To investigate the effect of the relationship between the average thickness of the landslide and the height of the bucket foundation (i.e., less than, equal to, and greater than) on the impact process, landslides with different initial thicknesses H have been investigated. It should be noted that the initial slope angle and bucket foundation distance remain constant, and the average thickness H' of the landslide at the moment of impact is subsequently determined. Results are shown in Figs. 14 and 15. It is observed that when the average thickness H' of the landslide at the moment of impact is smaller than the height of the bucket, increasing the initial thickness of the landslide (from 0.5 to 1.0 m) leads to an increase in the maximum instantaneous impact force and displacement response of the foundation. Conversely, when the average thickness of the landslide H' at the moment of impact is greater than the height of the bucket, increasing the initial thickness of the landslide (from 1.0 to 1.5 m) no longer has a significant influence on the maximum instantaneous impact force or the maximum displacement response of the bucket foundation (both about only 3% increase). However, the increased total volume and kinetic energy of the landslide prolong the impact force duration, resulting in a larger stable displacement of the bucket foundation (20% increase). Given that the stability of bucket foundations in extreme conditions is primarily assessed based on their displacement response, future research should pay more attention to this aspect.

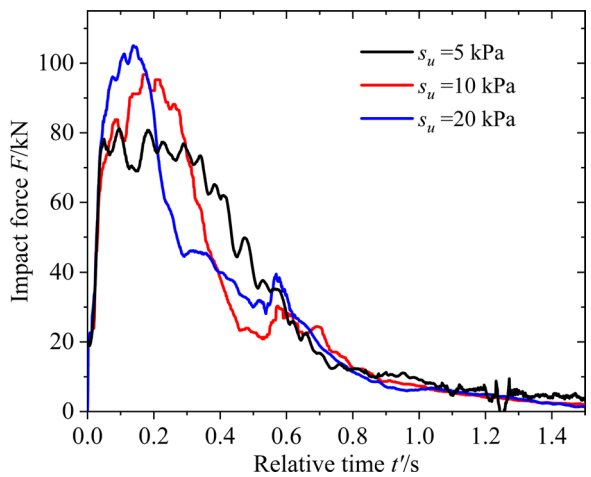

Fig. 16 Effect of different subgrade soil shear strength on the impact force

Effect of strength

Considering the uncertainty regarding the location of underwater landslides, a parametric analysis has been conducted for the undrained shear strength s_u of the subgrade soil, where s_u varies from 5 to 20 kPa. The initial velocity of the landslide body is set to 10 m/s (initial spacing is adjusted accordingly), and the model's other parameters are consistent with those described in 4.1. Figures 16 and 17 respectively illustrate the time-history curves for impact forces and bucket foundation displacement responses. It is evident that the increase in the undrained shear strength of the subgrade soil has no significant impact on the direct impact forces experienced by the bucket foundation. However, it notably influences the horizontal displacement of the bucket foundation when the impact force exceeds the subgrade's impact-bearing capacity limit. With the increase in subgrade soil strength (s_u ranging from 5 to 20 kPa), the maximum horizontal displacement of the bucket foundation

Content courtesy of Springer Nature, terms of use apply. Rights reserved.

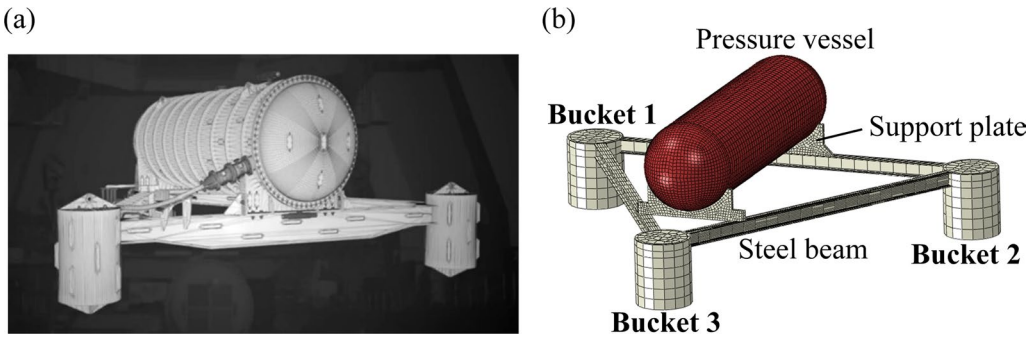

Fig. 18 Finite element model of the underwater data center; **a** full-size model of the Microsoft underwater data center (modified from Naval Group 2018); **b** the FEM model

changes from 24 mm to 0.2 m. Correspondingly, the foundation experiences instability, leading to overturning and failure under the impact. These findings further emphasize the advantages of the proposed method (SPH-FEM coupling method) in simulating fluid–structure coupling impact problems. It can model the interaction between the bucket and soil throughout the bidirectional fluid–structure impact, as well as quantify the dynamic displacement response of the bucket foundation during the impact process.

A case study: offshore landslides impact on the underwater data center

In offshore engineering, group bucket foundations are commonly employed for various purposes such as offshore wind turbines and underwater data centers. According to relevant reports (Simon 2018; Sutherland and Bopp 2023), Microsoft has successfully deployed an underwater data center using a three-bucket configuration (shown in Fig. 18a). The innovation offers advantages such as reduced energy consumption, lower carbon emissions, improved computer performance, and support for environmentally friendly and sustainable development of data centers. With the increasing demand for large-scale scientific computing, the establishment of underwater data centers has become a crucial strategic need requirement. Therefore, conducting numerical simulations on the impact of offshore landslide-induced on underwater data center foundations is crucial for optimizing the design of such infrastructures.

Modelling and simulated working conditions

The numerical underwater data center model consists of a steel pressure vessel, a steel frame (steel support plates, steel beams), and three steel bucket foundations. The upper part of the facility is the pressure vessel, with a total length of 12.2 m, an inner diameter of 2.8 m, an outer diameter of 3.18 m, and an average density of 2500 kg/m^3. The middle part of the facility is the steel beams' structure, measuring 14.3 m in length and 12.7 m in width. The steel beams each have a height of 500 mm, a width of 450 mm, a flange thickness of 25 mm, and a web plate thickness of 25 mm. The lower part of the facility consists of three connected bucket foundations. Each bucket is numbered, with a radius of 1.0 m, a burial depth of 2.0 m, and a total height of 2.5 m (shown in Fig. 18b). The subgrade adopts an elastoplastic constitutive model, as outlined in 4.1, and a grid size around the bucket of 0.01 m. All pertinent physical and mechanical parameters of the overlying water body, as well as the contact details within the model, remain consistent with those described in 4.1.

To account for the uncertainty of the landslide's impact direction, three directions with relatively large projected lengths (L_p) labeled A, B, and C are proposed, to investigate the effect of impact direction on the displacement response of the data center. The offshore landslide is assumed to have an initial thickness of 2 m, a slope angle of 45°, and an extension length of 50 m (three times more than L_p). The initial density of the landslide is $\rho = 1681$ kg/m^3, and the initial velocity is $v_0 = 10$ m/s. The characteristic length of the landslide's SPH particles is 0.05 m, while the characteristic length of the water particles is 0.1 m. Figure 19 depicts the results of the landslide impact on the underwater data center.

Results analysis and suggestions

Figure 19b reveals that in Direction A and B, both the maximum instantaneous impact force and the corresponding foundation displacement response are significantly larger compared to Direction C. The influence of directions on the maximum displacement response can reach up to 80%. The substantial volume of the landslide causes the maximum instantaneous impact force to exceed the bearing capacity of the foundation, resulting in instability failure of the group bucket foundation in all

Content courtesy of Springer Nature, terms of use apply. Rights reserved.

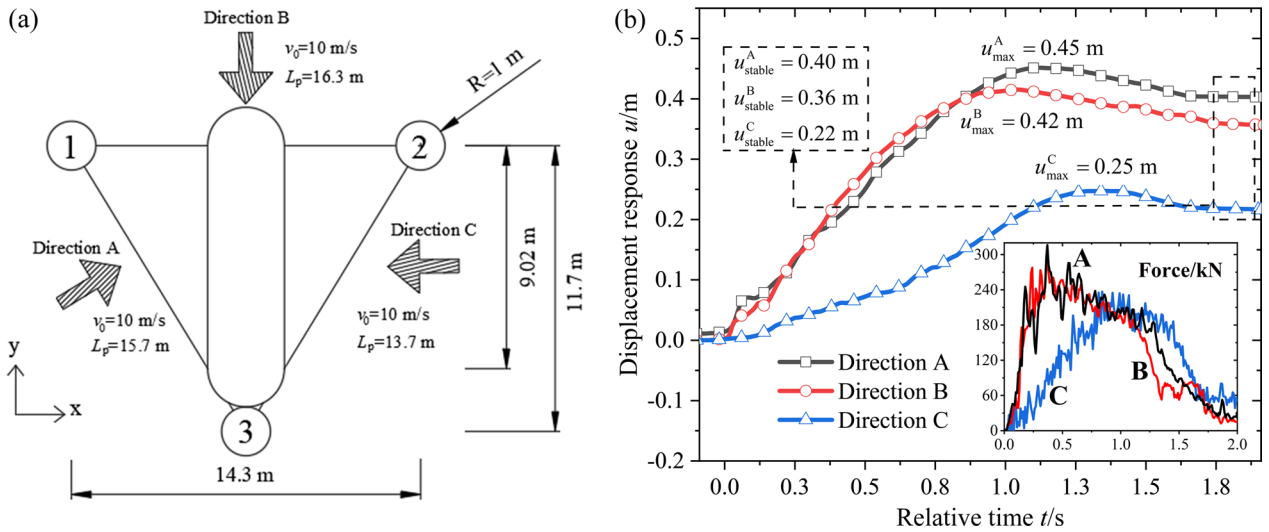

Fig. 19 Results of the landslide impact on the underwater data center; **a** three proposed impact directions; **b** impact force and displacement response time history curves

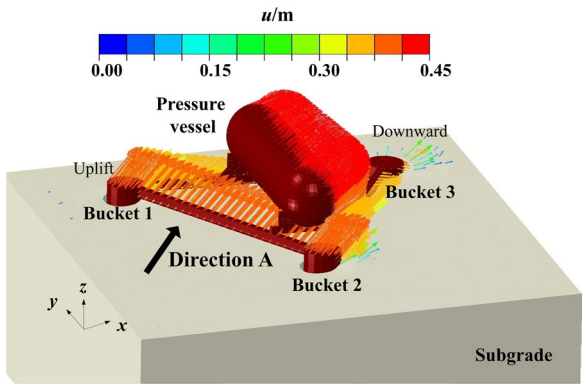

Fig. 20 Displacement response of data center under slide impact in Direction A at t = 2.0 s

cases. Additionally, the large size of the structure leads to inadequate flow around the landslide, prolonging the duration of the impact force compared to a single bucket and resulting in a greater displacement response. The group bucket foundation experiences a combined effect of horizontal forces and overturning moments from the landslide of Direction A, ultimately leading to combined translation-turnover failure, characterized by an uplift of Bucket 1 and 3 and a downward of Bucket 2, as shown in Fig. 20.

In the context of designing underwater data centers, it is essential to prioritize the assessment of the foundation's resistance under Direction A (i.e., when Bucket 1 and 3 or Bucket 2 and 3 are simultaneously subjected to forces). Special attention should be given to the deformation of the steel beams and the reliability of the steel frame to prevent connection failures caused by offshore landslides. Moreover, the efficient removal of deposited sediment from the impact flow is crucial for ensuring effective heat dissipation. It is worth noting that, due to the absence of detailed model specifics and on-site measurement data for underwater data centers, the aforementioned numerical simulations were conducted under several assumptions. Nonetheless, the proposed methods still aid in recognizing the most critical scenarios and the pattern of foundation instability and the qualitative conclusions derived can also serve as recommendations for the design of underwater data centers.

Conclusions

The impact of offshore landslides on underwater foundations was investigated using the proposed SPH-FEM method, focusing on analyzing the impact process and dynamic response of bucket foundations. The effects of the initial velocity, thickness, shear strength of subgrade and direction of the landslide on the impact of the bucket foundation and underwater data center were examined, leading to the following conclusions.

1. The proposed SPH-FEM method is well suited for simulating the submarine landslide impact on bucket foundations. In a single impact process, the impact force demonstrates a distinct decrease followed by stabilization, while the displacement response of

Content courtesy of Springer Nature, terms of use apply. Rights reserved.

the bucket foundation shows a rebound effect after reaching its maximum value.

2. Low-speed slides ($v_0 = 5$ m/s) exhibit blocking and accumulation behaviors, whereas high-speed slides ($v_0 = 20$ m/s) display a typical disperse behavior. The increase in thickness and shear strength of subgrade soil does not always affect the magnitude of the peak impact force directly, instead, it contributes to a larger stable displacement response.
3. The group-bucket foundations of the underwater data center undergo combined translation-turnover failure under the landslide impact. The impact direction of landslides also plays a significant role in the impact process. Specifically, Direction A represents the most unfavorable scenario for offshore landslide impact on the underwater data center.

Abbreviations

CFD	Computational fluid dynamics
FE	Finite element
FEM	Finite element method
MPM	Material point method
PMMA	Polymethyl methacrylate
SPH	Smoothed particle hydrodynamics

Acknowledgements
The authors thank all the scholars in the references for their contributions in their research fields.

Author contributions
ZW contributed to the implementation, software, and writing—original draft preparation. DZ contributed to the conceptualization and writing—review & editing. XG contributed to the modeling and writing—review & editing. ZG contributed to the writing—review & editing. YS contributed to the writing—review & editing. TN contributed to the conceptualization, design and writing—review & editing. The authors read and approved the final manuscript.

Funding
Funding for the research has been supported by the National Natural Science Foundation of China (42077272, 42377185 and 52079020), the LiaoNing Revitalization Talents Program (XLYC2002036), the open research fund program of Zhoushan Field Scientific Observation and Research Station for Marine Geo-hazards, China Geological Survey (No. ZSORS-22–04/09), and the Opening fund of State Key Laboratory of Coastal and Offshore Engineering at Dalian University of Technology (LP2310).

Availability of data and materials
All data, models, and code generated or used during the study appear in the submitted article.

Declarations

Competing interests
The authors declare that they have no competing interests.

Received: 14 July 2023 Accepted: 4 January 2024
Published online: 12 January 2024

References

Attaway SW, Heinstein MW, Swegle JW (1994) Coupling of smooth particle hydrodynamics with the finite element method. Nucl Eng Des 150(2–3):199–205. https://doi.org/10.1016/0029-5493(94)90136-8
Bea RG (1971) How sea floor slides affect offshore structures. Oil Gas J 69(48):88–92
Camargo JM, Silva MV, Ferreira Júnior AV, Araújo TC (2019) Marine geohazards: a bibliometric-based review. Geosciences 9(2):100. https://doi.org/10.3390/geosciences9020100
Campbell J, Vignjevic R, Libersky L (2000) A contact algorithm for smoothed particle hydrodynamics. Comput Methods Appl Mech Eng 184(1):49–65. https://doi.org/10.1016/S0045-7825(99)00442-9
Chen F, Yan H (2021) Constitutive model for solid-like, liquid-like, and gas-like phases of granular media and their numerical implementation. Powder Technol 390:369–386. https://doi.org/10.1016/j.powtec.2021.05.023
Coussot P, Laigle D, Arattano M, Deganutti A, Marchi L (1998) Direct determination of rheological characteristics of debris flow. J Hydraul Eng 124(8):865–868. https://doi.org/10.1061/(ASCE)0733-9429(1998)124:8(865)
Dai Z, Huang Y, Cheng H, Xu Q (2017) SPH model for fluid–structure interaction and its application to debris flow impact estimation. Landslides 14(3):917–928. https://doi.org/10.1007/s10346-016-0777-4
Dong Y, Wang D, Randolph MF (2017) Investigation of impact forces on pipeline by submarine landslide using material point method. Ocean Eng 146:21–28. https://doi.org/10.1016/j.oceaneng.2017.09.008
Dutta S, Hawlader B (2019) Pipeline–soil–water interaction modelling for submarine landslide impact on suspended offshore pipelines. Géotechnique 69(1):29–41. https://doi.org/10.1680/jgeot.17.P.084
El Talibi H, El Moussaoui S, Zaghloul MN, Aboumaria K, Wassmer P, Mercier JL (2016) New sedimentary and geomorphic evidence of tsunami flooding related to an older events along the Tangier-Asilah coastal plain, Morocco. Geoenviron Disasters 3:1–21. https://doi.org/10.1186/s40677-016-0049-6
Fan N, Zhang W, Sahdi F, Nian T (2022) Evaluation of horizontal submarine slide impact force on pipeline via a modified hybrid geotechnical–fluid dynamics framework. Can Geotech J 59(6):827–836. https://doi.org/10.1139/cgj-2021-0089
Feng R, Fourtakas G, Rogers BD, Lombardi D (2022) Two-phase fully-coupled smoothed particle hydrodynamics (SPH) model for unsaturated soils and its application to rainfall-induced slope collapse. Comput Geotech 151:104964. https://doi.org/10.1016/j.compgeo.2022.104964
Gao B, Ye G, Zhang Q, Xie Y, Yan B (2021) Numerical simulation of suction bucket foundation response located in liquefiable sand under earthquakes. Ocean Eng 235:109394. https://doi.org/10.1016/j.oceaneng.2021.109394
Guo X, Fan N, Liu Y, Liu X, Wang Z, Xie X, Jia Y (2023) Deep seabed mining: frontiers in engineering geology and environment. Int J Coal Sci Technol 10:23. https://doi.org/10.1007/s40789-023-00580-x
Guo X, Nian T, Fan N, Jia Y (2021) Optimization design of a honeycomb-hole submarine pipeline under a hydrodynamic landslide impact. Mar Georesour Geotechnol 39(9):1055–1070. https://doi.org/10.1080/1064119X.2020.1801919
Guo X, Nian T, Stoesser T (2022a) Using dimples to reduce submarine landslide impact forces on pipelines at different span heights. Ocean Eng 244:110343. https://doi.org/10.1016/j.oceaneng.2021.110343
Guo X, Stoesser T, Nian T, Jia Y, Liu X (2022b) Effect of pipeline surface roughness on peak impact forces caused by hydrodynamic submarine mudflow. Ocean Eng 243:110184. https://doi.org/10.1016/j.oceaneng.2021.110184
Guo X, Zheng D, Nian T, Yin P (2019) Effect of different span heights on the pipeline impact forces induced by deep-sea landslides. Appl Ocean Res 87:38–46. https://doi.org/10.1016/j.apor.2019.03.009
Hsu SK, Kuo J, Chung-Liang L, Ching-Hui T, Doo WB, Ku CY, Sibuet JC (2008) Turbidity currents, submarine landslides and the 2006 Pingtung earthquake off SW Taiwan. Terr Atmos Ocean Sci 19(6):7. https://doi.org/10.3319/TAO.2008.19.6.767(PT)
Huang Y, Zhu C (2015) Numerical analysis of tsunami–structure interaction using a modified MPS method. Nat Hazards 75:2847–2862. https://doi.org/10.1007/s11069-014-1464-1
Khalfaoui O, Dezileau L, Degeai JP, Snoussi M (2020) A late Holocene record of marine high-energy events along the Atlantic coast of Morocco: new

Content courtesy of Springer Nature, terms of use apply. Rights reserved.

evidences from the Tahaddart estuary. Geoenviron Disasters 7(1):1–14. https://doi.org/10.1186/s40677-020-00169-5
Korson L, Drost-Hansen W, Millero FJ (1969) Viscosity of water at various temperatures. J Phys Chem 73(1):34–39. https://doi.org/10.1021/j100721a006
Koshizuka S, Oka Y (1996) Moving-particle semi-implicit method for fragmentation of incompressible fluid. Nucl Sci Eng 123(3):421–434. https://doi.org/10.13182/NSE96-A24205
Lobovský L, Botia-Vera E, Castellana F, Mas-Soler J, Souto-Iglesias A (2014) Experimental investigation of dynamic pressure loads during dam break. J Fluids Struct 48:407–434. https://doi.org/10.1016/j.jfluidstructs.2014.03.009
Liang S, Chen Z (2019) SPH-FEM coupled simulation of SSI for conducting seismic analysis on a rectangular underground structure. Bull Earthq Eng 17:159–180. https://doi.org/10.1007/s10518-018-0456-z
Liu J, Tian J, Yi P (2015) Impact forces of submarine landslides on offshore pipelines. Ocean Eng 95:116–127. https://doi.org/10.1016/j.oceaneng.2014.12.003
Liu X, Wang Y, Zhang H, Guo X (2023) Susceptibility of typical marine geological disasters: an overview. Geoenviron Disasters 10(1):1–31. https://doi.org/10.1186/s40677-023-00237-6
Luo G, Pan S, Zhang Y, Chen L (2019) Response analysis of submerged floating tunnel hit by submarine based on smoothed-particle hydrodynamics. Shock Vib 2019:1–12. https://doi.org/10.1155/2019/9056416
Monaghan JJ (1992) Smoothed particle hydrodynamics. Ann Rev Astron Astrophys 30(1):543–574. https://doi.org/10.1146/annurev.aa.30.090192.002551
Monaghan JJ (1994) Simulating free surface flows with SPH. J Comput Phys 110(2):399–406. https://doi.org/10.1006/jcph.1994.1034
Monaghan JJ (2002) SPH compressible turbulence. Mon Not R Astron Soc 335(3):843–852. https://doi.org/10.1046/j.1365-8711.2002.05678.x
Naval Group (2018) Project Natick: Naval Group collaborates with Microsoft to deploy underwater Datacenter. France. https://www.youtube.com/watch?v=hSlaC_Tgvyl
Nian T, Guo X, Fan N, Jiao H, Li D (2018) Impact forces of submarine landslides on suspended pipelines considering the low-temperature environment. Appl Ocean Res 81:116–125. https://doi.org/10.1016/j.apor.2018.09.016
Nian T, Guo X, Zheng D, Xiu Z, Jiang Z (2019) Susceptibility assessment of regional submarine landslides triggered by seismic actions. Appl Ocean Res 93:101964. https://doi.org/10.1016/j.apor.2019.101964
Qian X, Liu Z, Xu J (2023) New insights into quantifying the stable impact forces of a submarine debris flow on a pipeline. Ocean Eng 274:114060. https://doi.org/10.1016/j.oceaneng.2023.114060
Qian X, Xu J, Bai Y, Das HS (2020) Formation and estimation of peak impact force on suspended pipelines due to submarine debris flow. Ocean Eng 195:106695. https://doi.org/10.1016/j.oceaneng.2019.106695
Shano L, Raghuvanshi TK, Meten M (2020) Landslide susceptibility evaluation and hazard zonation techniques—a review. Geoenviron Disasters 7(1):1–19. https://doi.org/10.1186/s40677-020-00152-0
Shi X, Xu R, Gong X, Chen G, Yuan Z (1999) Experimental study on horizontal bearing capacity of single bucket foundation. Chin J Geotech Eng 06:723–726 (**in Chinese**)
Simon K (2018) Project Natick-Microsoft's self-sufficient underwater datacenters. IndraStra Global 4(6):4
Sun Y, Bolin H (2014) A potential tsunami impact assessment of submarine landslide at Baiyun Depression in Northern South China Sea. Geoenviron Disasters 1(1):1–11. https://doi.org/10.1186/s40677-014-0007-0
Sutherland T, Bopp G (2023) The Pacific futures of subsea data centers. New Media Soc 25(2):345–360. https://doi.org/10.1177/1461444822114994
Ucar Y, Akova T, Aysan I (2012) Mechanical properties of polyamide versus different PMMA denture base materials. J Prosthodont Implant Esthetic Reconstr Dent 21(3):173–176. https://doi.org/10.1111/j.1532-849X.2011.00804.x
Wang Z, Sun Y, Jia Y, Shan Z, Shan H, Zhang S, Wen M, Liu X, Song Y, Zhao D, Wen S (2020) Wave-induced seafloor instabilities in the subaqueous Yellow River Delta—initiation and process of sediment failure. Landslides 17:1849–1862. https://doi.org/10.1007/s10346-020-01399-2
Xu F, Kikuchi M (2005) The study of kernel functions in impact problem simulation by using SPH method. Int J Comput Methods 2(04):587–600. https://doi.org/10.1142/S0219876205000612
Zakeri A, Høeg K, Nadim F (2008) Submarine debris flow impact on pipelines—Part I: experimental investigation. Coast Eng 55(12):1209–1218. https://doi.org/10.1016/j.coastaleng.2008.06.003
Zakeri A, Høeg K, Nadim F (2009) Submarine debris flow impact on pipelines—part II: numerical analysis. Coast Eng 56(1):1–10. https://doi.org/10.1016/j.coastaleng.2008.06.005
Zhan L, Peng C, Zhang B, Wu W (2020) A SPH framework for dynamic interaction between soil and rigid body system with hybrid contact method. Int J Numer Anal Methods Geomech 44(10):1446–1471. https://doi.org/10.1002/nag.3070
Zhang W, Zheng H, Jiang F, Wang Z, Gao Y (2019) Stability analysis of soil slope based on a water–soil-coupled and parallelized Smoothed Particle Hydrodynamics model. Comput Geotech 108:212–225. https://doi.org/10.1016/j.compgeo.2018.12.025
Zhao E, Dong Y, Tang Y, Cui L (2021) Numerical study on hydrodynamic load and vibration of pipeline exerted by submarine debris flow. Ocean Eng 239:109754. https://doi.org/10.1016/j.oceaneng.2021.109754
Zheng D, Lei D, Yan C, Shen Y, Nian T (2021) Global research trends in submarine landslides: a bibliometric analysis based on Web of Science publications. J Eng Geol 29(6):1805–1814. https://doi.org/10.13544/j.cnki.jeg.2021-0712. (**in Chinese**)
Zhu C, Fei Q (2022) Impact characteristics and strength evaluation of a slender body obliquely entering water at high speed. J Phys Conf Ser 2338(1):012–024. https://doi.org/10.1088/1742-6596/2338/1/012024
Zhu C, Chen Z, Huang Y (2021) Coupled moving particle simulation–finite-element method analysis of fluid–structure interaction in geodisasters. Int J Geomech 21(6):04021081. https://doi.org/10.1061/(ASCE)GM.1943-5622.0002041

Publisher's Note

Springer Nature remains neutral with regard to jurisdictional claims in published maps and institutional affiliations.

Submit your manuscript to a SpringerOpen journal and benefit from:

- ► Convenient online submission
- ► Rigorous peer review
- ► Open access: articles freely available online
- ► High visibility within the field
- ► Retaining the copyright to your article

Submit your next manuscript at ► springeropen.com

Content courtesy of Springer Nature, terms of use apply. Rights reserved.

Terms and Conditions

Springer Nature journal content, brought to you courtesy of Springer Nature Customer Service Center GmbH (“Springer Nature”).
Springer Nature supports a reasonable amount of sharing of research papers by authors, subscribers and authorised users (“Users”), for small-scale personal, non-commercial use provided that all copyright, trade and service marks and other proprietary notices are maintained. By accessing, sharing, receiving or otherwise using the Springer Nature journal content you agree to these terms of use (“Terms”). For these purposes, Springer Nature considers academic use (by researchers and students) to be non-commercial.
These Terms are supplementary and will apply in addition to any applicable website terms and conditions, a relevant site licence or a personal subscription. These Terms will prevail over any conflict or ambiguity with regards to the relevant terms, a site licence or a personal subscription (to the extent of the conflict or ambiguity only). For Creative Commons-licensed articles, the terms of the Creative Commons license used will apply.
We collect and use personal data to provide access to the Springer Nature journal content. We may also use these personal data internally within ResearchGate and Springer Nature and as agreed share it, in an anonymised way, for purposes of tracking, analysis and reporting. We will not otherwise disclose your personal data outside the ResearchGate or the Springer Nature group of companies unless we have your permission as detailed in the Privacy Policy.
While Users may use the Springer Nature journal content for small scale, personal non-commercial use, it is important to note that Users may not:

1. use such content for the purpose of providing other users with access on a regular or large scale basis or as a means to circumvent access control;
2. use such content where to do so would be considered a criminal or statutory offence in any jurisdiction, or gives rise to civil liability, or is otherwise unlawful;
3. falsely or misleadingly imply or suggest endorsement, approval , sponsorship, or association unless explicitly agreed to by Springer Nature in writing;
4. use bots or other automated methods to access the content or redirect messages
5. override any security feature or exclusionary protocol; or
6. share the content in order to create substitute for Springer Nature products or services or a systematic database of Springer Nature journal content.

In line with the restriction against commercial use, Springer Nature does not permit the creation of a product or service that creates revenue, royalties, rent or income from our content or its inclusion as part of a paid for service or for other commercial gain. Springer Nature journal content cannot be used for inter-library loans and librarians may not upload Springer Nature journal content on a large scale into their, or any other, institutional repository.
These terms of use are reviewed regularly and may be amended at any time. Springer Nature is not obligated to publish any information or content on this website and may remove it or features or functionality at our sole discretion, at any time with or without notice. Springer Nature may revoke this licence to you at any time and remove access to any copies of the Springer Nature journal content which have been saved.
To the fullest extent permitted by law, Springer Nature makes no warranties, representations or guarantees to Users, either express or implied with respect to the Springer nature journal content and all parties disclaim and waive any implied warranties or warranties imposed by law, including merchantability or fitness for any particular purpose.
Please note that these rights do not automatically extend to content, data or other material published by Springer Nature that may be licensed from third parties.
If you would like to use or distribute our Springer Nature journal content to a wider audience or on a regular basis or in any other manner not expressly permitted by these Terms, please contact Springer Nature at

onlineservice@springernature.com